Front. Mech. Eng. 2014, 9(4): 295–307
DOI 10.1007/s11465-014-0317-7

RESEARCH ARTICLE

Jingjun YU, Dengfeng LU, Zhongxiang ZHANG, Xu PEI

Motion capability analysis of a quadruped robot as a parallel manipulator

Abstract This paper presents the forward and inverse displacement analysis of a quadruped robot MANA as a parallel manipulator in quadruple stance phase, which is used to obtain the workspace and control the motion of the body. The robot MANA designed on the basis of the structure of quadruped mammal is able to not only walk and turn in the uneven terrain, but also accomplish various manipulating tasks as a parallel manipulator in quadruple stance phase. The latter will be the focus of this paper, however. For this purpose, the leg kinematics is primarily analyzed, which lays the foundation on the gait planning in terms of locomotion and body kinematics analysis as a parallel manipulator. When all four feet of the robot contact on the ground, by assuming there is no slipping at the feet, each contacting point is treated as a passive spherical joint and the kinematic model of parallel manipulator is established. The method for choosing six non-redundant actuated joints for the parallel manipulator from all twelve optional joints is elaborated. The inverse and forward displacement analysis of the parallel manipulator is carried out using the method of coordinate transformation. Finally, based on the inverse and forward kinematic model, two issues on obtaining the reachable workspace of parallel manipulator and planning the motion of the body are implemented and verified by ADAMS simulation.

Keywords quadruped robot, actuated joints selection, kinematics analysis, motion planning, parallel manipulator

1 Introduction

Legged robots are able to adapt to various road conditions and thus have an excellent motion performance because they have redundant structures and multiple degrees of freedom (DOFs). More and more legged robots are used to fulfill some specific tasks instead of human beings in the complex or dangerous environment. In the family of legged robots, a quadruped robot, due to its good motion stability and relatively simple mechanical structure, increasingly becomes the focus of current robotics research.

In recent years, great progress has been made on study of quadruped robots [1–4]. Japanese scholars developed the robot Tekken series [5], in which the central pattern generator (CPG) and reflexes are used to realize adaptive dynamic walking of the robot on irregular terrain. Boston Dynamics Incorporation (BDI) developed the compact quadruped robot — LittleDog [6], which is used to study the relationship among motor learning, dynamic control, perception of the environment and rough-terrain locomotion. So far, the most representative quadruped robot is another robot BigDog [7] developed by BDI. It can travel in outdoor tough terrain such as steep, rutted, rocky, wet, muddy and snowy environment.

However, the current quadruped robot research is mainly centralized in mechanism design, gait planning, control algorithm, locomotion analysis and so on. In particular, more attentions have been paid on the locomotion of the quadruped robot, such as walking, running and turning. While the motion capability analysis of the four-legged robot as a parallel manipulator in quadruple stance phase is rarely discussed. As well known, a puppy must eat and scratch in addition to running around. So the motion capability of the quadruped robot cannot be only limited to the locomotion and should extend to manipulation capability analysis as a parallel manipulator. Ren and Hong [8] have carried out triple stance phase displacement analysis in a three-legged mobile robot (STriDER) using parallel kinematics. However, the object of the study is a three-legged robot which lacks motion stability. Besides, the whole research doesn't refer to how to rationally select actuators for the parallel mechanism and obtain the desired workspace.

Received October 7, 2014; accepted November 11, 2014

Jingjun YU (✉), Dengfeng LU, Zhongxiang ZHANG, Xu PEI
School of Mechanical Engineering & Automation, Beihang University, Beijing 100191, China
E-mail: jjyu@buaa.edu.cn

Therefore, the main objective of this paper is to implement the motion capability analysis of a quadruped robot as a parallel manipulator. A quadruped robot named MANA is firstly introduced. MANA can be modeled as a four-limb parallel manipulator in the quadruple stance phase, and the contact between each foot and the ground is regarded as a pure rolling. In terms of its product-of-exponential (POE)-based kinematic model, both inverse and forward displacement analysis is presented, which is applied to obtain the workspace and plan the motion of the body.

The whole paper is organized as follows: Section 2 characterizes the geometrical parameters of the robot MANA; Section 3 introduces the displacement analysis of a single leg, which is the foundation of displacement analysis for the body of MANA; Section 4 proposes the method of choosing six non-redundant actuated joints for MANA and formulates the inverse and forward displacement, which is used to obtain the reachable workspace and plan motion of the body; Section 5 implements the motion capability analysis and simulation of the robot MANA as a parallel manipulator based on the kinematic analysis and the virtual prototype; finally, Section 6 summarizes all concluded results.

2 Description of the quadruped robot MANA

As shown in Fig. 1, a quadruped robot named MANA is designed according to mammalian body structure, and its structural diagram is illustrated in Fig. 2. The quadruped robot consists of four legs and one body, and each leg has three revolute joints connecting in series. All structural parameters of the robot have been listed in Table 1. Note that the hip 1 joint axis is located along the horizontal direction of X-axis while the hip 2 and knee joint axes are distributed both along the side direction of Y-axis.

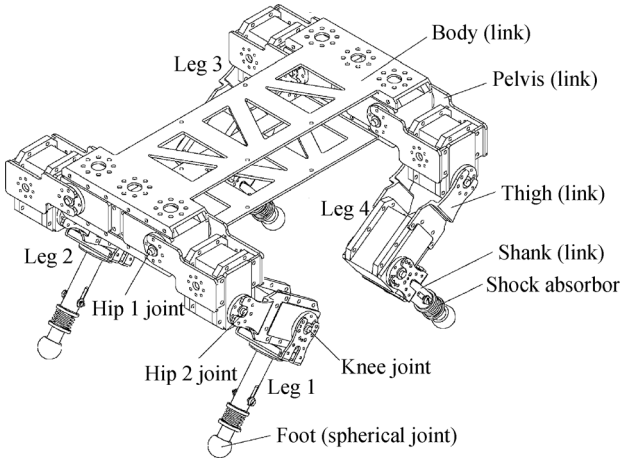

Fig. 1 A quadruped robot MANA

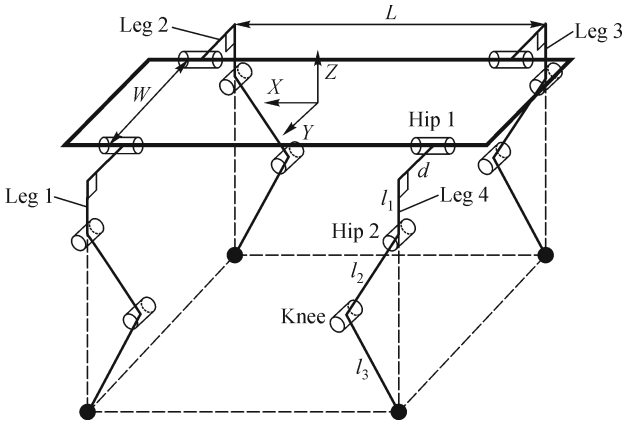

Fig. 2 Structural diagram of the robot MANA

Table 1 Structural parameters of MANA robot

Structural parameter	Value/mm
L (Body length)	210
W (Body width)	160
H (Body height)	210
d (Pelvis width)	30
l_1 (Pelvis length)	40
l_2 (Thigh length)	75
l_3 (Shank length)	105
S (Displacement)	5
D (Diameter of robot feet)	15

The research on the locomotion of the quadruped robot MANA can be found in Ref. [9]. This paper will focus on motion capability analysis of the quadruped robot as a parallel manipulator. MANA can be modeled as a four-limb in-parallel manipulator when it stays in the quadruple stance phase, all four feet contact points are treated as passive spherical joints (S). The kinematic model of the four-limb parallel manipulator will be established in Section 4.

3 Leg kinematics based on POE formula

Before the motion capability analysis of the parallel manipulator is carried out, it is necessary to fulfill kinematic analysis of the parallel manipulator. However, leg kinematics must be preferred to be modelled before the kinematic analysis of the parallel manipulator is conducted. In this paper, each leg is regarded as an open-chain serial manipulator and the leg kinematics is formulated based on the POE formula of Screw Theory [10].

3.1 Forward displacement analysis

The forward displacement analysis requires determining the position and orientation of foot given the information

about the joint angles. The body of the robot is modeled as "the base" of the serial manipulator, and the foot as "the end effector". At the initial posture shown in Fig. 3(a), the link with the length of l_1, the link with the length of l_2 and the link with the length of l_3 are collinear with each other; the link with the length of d are parallel to the middle plane of the body. At the general posture shown in Fig. 3(b), hip 1 joint, hip 2 joint and knee joint all rotate around a certain angle. The definition of two coordinate systems can be also found in Fig. 3. One is a global coordinate system, {S}, which is established with its origin at the center of the hip 1 joint, whose X-axis is overlapping the hip 1 joint axis and Y-axis is parallel to the middle plane of the body. The other is a tool coordinate system {T}, which is obtained by translating global coordinate system {S} from point A to point B.

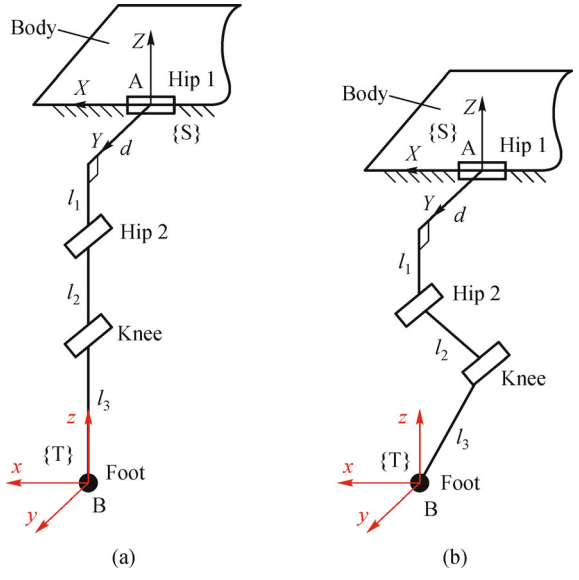

Fig. 3 Leg posture and coordinate frames. (a) Initial posture; (b) general posture

According to the POE formula [10], the transformation matrix from the tool coordinate system to the global one at a general configuration can be written as

$$g_{ST}(\boldsymbol{\theta}) = e^{\theta_1\hat{\xi}_1}e^{\theta_2\hat{\xi}_2}e^{\theta_3\hat{\xi}_3}g_{ST}(0) = \begin{bmatrix} \boldsymbol{R}(\boldsymbol{\theta}) & \boldsymbol{P}(\boldsymbol{\theta}) \\ 0 & 1 \end{bmatrix} \quad (1)$$

where θ_1, θ_2 and θ_3 are the angular displacements of hip 1 joint, hip 2 joint and knee joint, respectively; and

$$\boldsymbol{R}(\boldsymbol{\theta}) = \begin{bmatrix} \cos(\theta_2+\theta_3) & 0 & \sin(\theta_2+\theta_3) \\ \sin\theta_1\sin(\theta_2+\theta_3) & \cos\theta_1 & -\sin\theta_1\cos(\theta_2+\theta_3) \\ -\cos\theta_1\sin(\theta_2+\theta_3) & \sin\theta_1 & \cos\theta_1\cos(\theta_2+\theta_3) \end{bmatrix}$$

$$\boldsymbol{P}(\boldsymbol{\theta}) = \begin{bmatrix} -l_3\sin(\theta_2+\theta_3)-l_2\sin\theta_2 \\ d\cos\theta_1+\sin\theta_1\left(l_1+l_2\cos\theta_2+l_3\cos(\theta_2+\theta_3)\right) \\ d\sin\theta_1-\cos\theta_1\left(l_1+l_2\cos\theta_2+l_3\cos(\theta_2+\theta_3)\right) \end{bmatrix}$$

The process of obtaining Eq. (1) can be found in Ref. [9]. According to Eq. (1), the position and orientation of foot can be calculated in terms of the three given joint angles.

3.2 Inverse displacement analysis

The inverse displacement analysis is to calculate the unknown angles θ_1, θ_2 and θ_3 for hip 1, hip 2 and knee joints, respectively, as given a position of the foot.

If $\boldsymbol{P}(\boldsymbol{\theta}) = \begin{bmatrix} P_x & P_y & P_z \end{bmatrix}^{\mathrm{T}}$, it can be derived from Eq. (1) as

$$\begin{cases} P_x = -l_3\sin(\theta_2+\theta_3)-l_2\sin\theta_2 \\ P_y = d\cos\theta_1+\sin\theta_1\left(l_1+l_2\cos\theta_2+l_3\cos(\theta_2+\theta_3)\right) \\ P_z = d\sin\theta_1-\cos\theta_1\left(l_1+l_2\cos\theta_2+l_3\cos(\theta_2+\theta_3)\right) \end{cases} \quad (2)$$

According to Eq. (2), the angle at the hip 1 joint, θ_1, is obtained as

$$\theta_1 = 2\arctan\left(\frac{P_z \pm \sqrt{P_y^2+P_z^2-d^2}}{d+P_y}\right) \quad (3)$$

In the case of $\theta_1 \neq 90°$, the angle at the knee joint, θ_3, is calculated as

$$\theta_3 = \pm\arccos\left(\frac{D^2+P_x^2-l_2^2-l_3^2}{2l_2l_3}\right) \quad (4)$$

where $D = \dfrac{-P_z}{\cos\theta_1}+d\tan\theta_1-l_1$.

In the case of $\theta_1 = 90°$, the knee joint θ_3 is determined by

$$\theta_3 = \pm\arccos\left(\frac{C^2+P_x^2-l_2^2-l_3^2}{2l_2l_3}\right) \quad (5)$$

where $C = P_y-l_1$.

From Eq. (2), the angle at hip 2 joint, θ_2, is obtained as

$$\theta_2 = 2\arctan\left(\frac{A \pm \sqrt{B^2+A^2-P_x^2}}{B-P_x}\right) \quad (6)$$

where $A = l_2+l_3\cos\theta_3$, $B = l_3\sin\theta_3$.

According to Eqs. (3)–(6), the unknown angles θ_1, θ_2

and θ_3 for hip 1, hip 2 and knee joints can be calculated from a given position of the foot. However, the angles θ_1, θ_2 and θ_3 have a limited range of angular displacement when considering physical structure of the quadruped robot. The angle θ_1 subjects to $\theta_1 \in (-90°,90°)$, the angle θ_2 subjects to $\theta_2 \in (-180°,180°)$, and the angle θ_3 subjects to $\theta_3 \in (-180°,180°)$. Note that all these three angular ranges are resulted from the theoretical analysis in terms of the structural design parameters for the robot. As for the experimental prototype of the robot, however, all the ranges of angular displacement are even smaller considering the interference of the parts.

On the basis of the inverse displacement analysis and the angle range of each joint, it is concluded that there are two inverse displacement solutions. Of the two solutions, the one that has a smaller difference from the initial angles is chosen.

4 Body kinematics

4.1 Inverse displacement analysis

In the quadruple stance phase, MANA can be regarded as a four-limb parallel manipulator given the assumption that all four contacting points are fixed on the ground, as shown in Fig. 4. Since the position of each foot does not change and the link can rotate around the contacting point freely, the point contact between the rigid foot tip and the ground is modeled as a passive spherical joint [8]. The ground is modeled as "the base" of the parallel manipulator, with the body as "the moving platform" and the leg as "the limb". According to the conventional naming rules of parallel mechanisms, the configuration of MANA is indeed a 4-SRRR (S: spherical joint; R: rotational joint) parallel manipulator. As discussed in Ref. [9], the parallel manipulator has 6 DOFs. If a gripper is mounted on the body, the gripper can be used to grip objects.

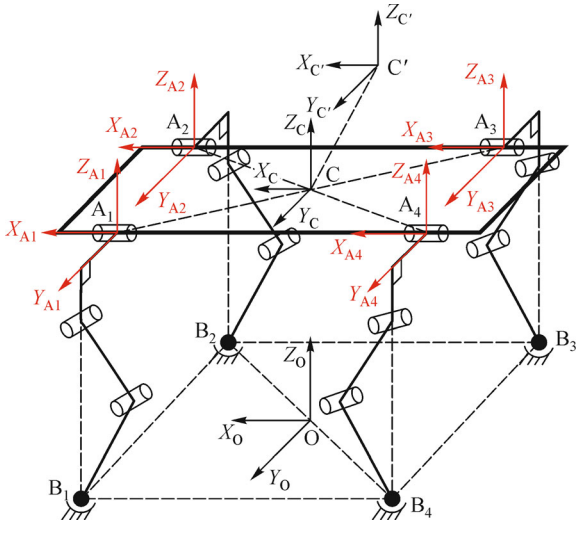

Fig. 4 Four-limb parallel manipulator and coordinate frames

The definition of all coordinate systems for the parallel manipulator is illustrated in Fig. 4. Firstly, the body coordinate system, $\{X_C, Y_C, Z_C\}$, is established with its origin at the center of the body, axis X_C parallel to the line A_4A_1, and axis Y_C parallel to the line A_2A_1. Next, a global coordinate system, $\{X_O, Y_O, Z_O\}$, is built with its origin at the center of the line B_2B_4. Three unit vectors $\boldsymbol{x}_o$, $\boldsymbol{y}_o$, and $\boldsymbol{z}_o$ along X_O, Y_O, and Z_O axis direction can be calculated as

$$\boldsymbol{x}_o = \frac{\overrightarrow{B_4B_1}}{\left|\overrightarrow{B_4B_1}\right|},\ \boldsymbol{z}_o = \frac{\overrightarrow{OB_1} \times \overrightarrow{OB_4}}{\left|\overrightarrow{OB_1} \times \overrightarrow{OB_4}\right|},\ \boldsymbol{y}_o = \frac{\boldsymbol{z}_o \times \boldsymbol{x}_o}{|\boldsymbol{z}_o \times \boldsymbol{x}_o|} \quad (7)$$

Finally, the leg i coordinate system, $\{X_{A_i}, Y_{A_i}, Z_{A_i}\}$, is obtained by translating the body coordinate system, $\{X_C, Y_C, Z_C\}$, from point C to point A_i, where i ($i = 1, 2, 3, 4$) denotes the number of legs.

When MANA changes the position and the orientation of its body without moving, the motion can be formulated in terms of parallel kinematics. As the center of the body moves from point C to point C′, the coordinate system fixed on the body changes from one frame $\{X_C, Y_C, Z_C\}$ to another one $\{X_{C'}, Y_{C'}, Z_{C'}\}$. The inverse displacement analysis is to calculate the unknown joint angles of each leg under the conditions that both the coordinate systems $\{X_C, Y_C, Z_C\}$ and $\{X_{C'}, Y_{C'}, Z_{C'}\}$ are known.

The location of the contacting point B_i with respect to the frame $\{X_O, Y_O, Z_O\}$ can be calculated as

$$\begin{pmatrix} {}^{O}\boldsymbol{P}_{B_i} \\ 1 \end{pmatrix} = {}^{O}\boldsymbol{T}_{C} \cdot {}^{C}\boldsymbol{T}_{A_i} \begin{pmatrix} {}^{A_i}\boldsymbol{P}_{B_i} \\ 1 \end{pmatrix} \quad (8)$$

where ${}^{O}\boldsymbol{T}_{C}$ is the transformation matrix from the body frame $\{X_C, Y_C, Z_C\}$ to the global frame $\{X_O, Y_O, Z_O\}$; ${}^{C}\boldsymbol{T}_{A_i}$ is the transformation matrix from the leg frame $\{X_{A_i}, Y_{A_i}, Z_{A_i}\}$ to the body frame $\{X_C, Y_C, Z_C\}$; and ${}^{A_i}\boldsymbol{P}_{B_i}$ is the location of the contacting point B_i with respect to the frame $\{X_{A_i}, Y_{A_i}, Z_{A_i}\}$.

The location of the contacting point B_i with respect to the frame $\{X_O, Y_O, Z_O\}$ can also be calculated by

$$\begin{pmatrix} {}^{O}\boldsymbol{P}_{B_i} \\ 1 \end{pmatrix} = {}^{O}\boldsymbol{T}_{C} \cdot {}^{C}\boldsymbol{T}_{C'} \cdot {}^{C'}\boldsymbol{T}_{A_{i'}} \begin{pmatrix} {}^{A'_i}\boldsymbol{P}_{B_i} \\ 1 \end{pmatrix} \quad (9)$$

where ${}^{C}\boldsymbol{T}_{C'}$ is the transformation matrix from the new body coordinates $\{X_{C'}, Y_{C'}, Z_{C'}\}$ to the initial body coordinates $\{X_C, Y_C, Z_C\}$; ${}^{C'}\boldsymbol{T}_{A_{i'}}$ is the transformation matrix from the new leg frame $\{X_{A'_i}, Y_{A'_i}, Z_{A'_i}\}$ to the new body frame $\{X_{C'}, Y_{C'}, Z_{C'}\}$. Furthermore, ${}^{C'}\boldsymbol{T}_{A_{i'}} = {}^{C}\boldsymbol{T}_{A_i}$, because the position and orientation of the body frame with respect to the leg frame is not changed as the position and orientation of the body frame with respect to the global frame change. ${}^{A_i}\boldsymbol{P}_{B_i}$ is the location of the contacting point B_i in the frame $\{X_{A'_i}, Y_{A'_i}, Z_{A'_i}\}$.

Note that the expression on the left of Eqs. (8) and (9) are identical, thus

$$
{}^{\mathrm{O}}\boldsymbol{T}_{\mathrm{C}} \cdot {}^{\mathrm{C}}\boldsymbol{T}_{\mathrm{A}_i} \begin{pmatrix} {}^{\mathrm{A}_i}\boldsymbol{P}_{\mathrm{B}_i} \\ 1 \end{pmatrix}
= {}^{\mathrm{O}}\boldsymbol{T}_{\mathrm{C}} \cdot {}^{\mathrm{C}}\boldsymbol{T}_{\mathrm{C}'} \cdot {}^{\mathrm{C}'}\boldsymbol{T}_{\mathrm{A}_i'} \begin{pmatrix} {}^{\mathrm{A}_i'}\boldsymbol{P}_{\mathrm{B}_i} \\ 1 \end{pmatrix} \tag{10}
$$

From Eq. (10), the location of the contact point B_i in the frame $\{X_{\mathrm{A}_i'}, Y_{\mathrm{A}_i'}, Z_{\mathrm{A}_i'}\}$ can be derived as

$$
\begin{pmatrix} {}^{\mathrm{A}_i'}\boldsymbol{P}_{\mathrm{B}_i} \\ 1 \end{pmatrix}
= ({}^{\mathrm{C}}\boldsymbol{T}_{\mathrm{A}_i})^{-1} \cdot ({}^{\mathrm{C}}\boldsymbol{T}_{\mathrm{C}'})^{-1} \cdot {}^{\mathrm{C}}\boldsymbol{T}_{\mathrm{A}_i} \begin{pmatrix} {}^{\mathrm{A}_i}\boldsymbol{P}_{\mathrm{B}_i} \\ 1 \end{pmatrix} \tag{11}
$$

where ${}^{\mathrm{C}}\boldsymbol{T}_{\mathrm{A}_i}$ is determined by the body size; ${}^{\mathrm{A}_i}\boldsymbol{P}_{\mathrm{B}_i}$ is determined by the initial posture of the body. Therefore, the vector ${}^{\mathrm{A}_i'}\boldsymbol{P}_{\mathrm{B}_i}$ can be calculated if the matrix ${}^{\mathrm{C}}\boldsymbol{T}_{\mathrm{C}'}$ is known. Thus the three joint angles of each leg can be calculated easily according to the inverse displacement analysis of the leg in Section 3.2.

4.2 Forward displacement analysis

As the foundation of obtaining the workspace of the body and conducting accuracy analysis, the forward displacement analysis requires solving the position and orientation of the body, as given all displacement information about the actuated joints. According to the knowledge of theory of machines and mechanisms, the parts of the mechanisms may be damaged under the condition that the number of actuators is larger than its DOFs.

Considering that the parallel manipulator has 6 DOFs and 12 optional actuators, it is necessary to select 6 non-redundant actuators from these 12 optional actuators.

4.2.1 Proper actuator selection

Proper actuator selection of the parallel manipulator refers to choose 6 non-redundant actuated joints from the all 12 optional actuated joints. Two principles when choosing 6 non-redundant actuated joints should be followed:

(I) If angles of the selected six actuated joints are constant, the moving platform will not move;

(II) The number of DOFs of the mechanism is independent of its configuration.

According to Principle (I), it is easy to find 6 non-redundant actuated joints at a certain configuration (such as the configuration shown in Fig. 5). Based on Principle (II), the selected six actuated joints using Principle (I) are still non-redundant as the body configuration changes.

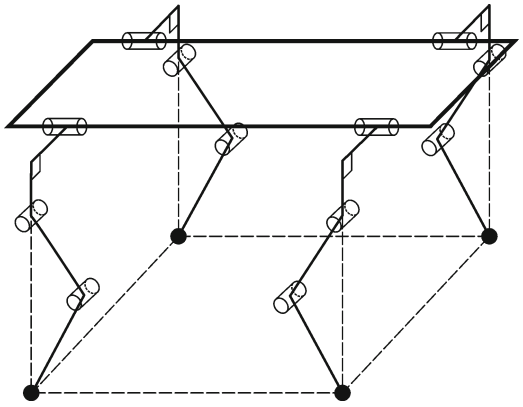

Fig. 5 A general configuration of the parallel manipulator

In the following section, constraint analysis of the moving platform provided by all four limbs in term of different actuator combinations are implemented, in which the two links connecting to actuated joint are regarded as one link.

The configurations for all four legs of MANA are identical, thus the analysis for one leg is present here, as the other three legs will follow the same procedure. For each leg, there are 8 cases of actuated joint combinations because each of the three joints is either "actuated joint" or "passive joint". In the case that none of the three joints is actuated joint, the limb provides no constraints to the moving platform. In the other seven cases, constraints of the platform provided by the limb are shown in Table 2.

In Table 2, all constraints are expressed by lines using freedom and constraint topology (FACT) [11] and the solid blue lines denote the constraint lines. For example, Case 1 in Table 2 means that the constraints of the moving platform provided by the limb are three spatial constraint lines intersecting at the center of the foot. The detailed knowledge about FACT is elaborated in Ref. [11].

For the robot MANA, the total number of actuated joints is 6 and each leg has at most 3 actuated joints. Now we need to distribute these six actuators in a rational way. In other words, how many actuated joints each leg exactly has. The nomenclature "$n_1 + n_2 + n_3 + n_4$" will be used to describe actuator distribution where n_1 corresponds to the number of actuated joints in leg i. For example, "$3 + 2 + 0 + 1$" means there are three actuated joints in leg 1, two actuated joints in leg 2, zero actuated joint in leg 3 and one actuated joint in leg 4.

Based on the previous two principles, some feasible combinations of actuated joints are enumerated, as shown in Table 3. Note that in the case that only three legs have actuated joints, leg 1, leg 2 and leg 4 are selected in preference. "Joint 3(2)" in Table 3 means either Joint 3 or Joint 2 is actuated joint, but Joint 3 is prior to be selected.

For example, in Table 3, the combination of actuated joints labeled in gray means that hip 1, hip 2 and knee joints in leg 1 are actuated joints; hip 2 and knee joints in

Table 2 Constraint distribution of the moving platform provided by the limb

Actuated joints	Joints 1, 2 and 3	Joints 2 and 3	Joints 1 and 3	Joints 1 and 2
Constraints of the moving platform provided by the limb	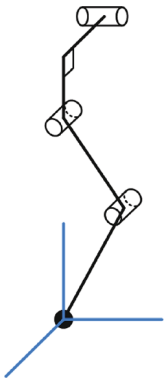	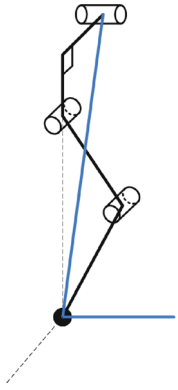	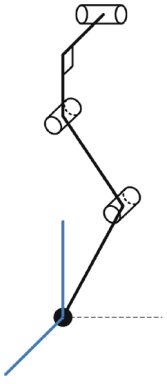	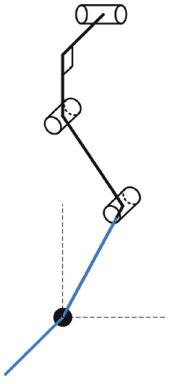

Actuated joints	Joint 1	Joint 2	Joint 3
Constraints of the moving platform provided by the limb	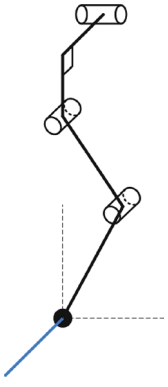	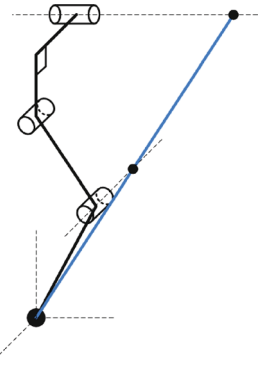	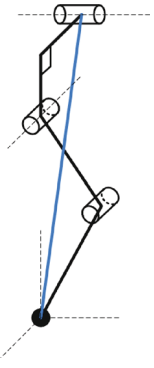

Note: Joints 1, 2 and 3 in Table 2 denote hip 1 joint, hip 2 joint and knee joint, respectively.

Table 3 Some feasible combinations for actuated joints

Distributions of actuators	Actuated joints of each leg			
	Leg 1	Leg 2	Leg 3	Leg 4
3 + 3 + 0 + 0	No feasible combinations			
3 + 2 + 0 + 1	Joints 1, 2 and 3	Joint 3(2)	–	Joints 1 and 3(2)
	Joints 1, 2 and 3	Joints 2 and 3		Joint 3(2)
3 + 1 + 1 + 1	Joints 1, 2 and 3	Joint 3(2)	Joint 3(2)	Joint 1
2 + 2 + 0 + 2	Joints 1 and 3(2)	Joints 2 and 3	–	Joints 1 and 3(2)
	Joints 2 and 3	Joints 2 and 3	–	Joints 1 and 3(2)
2 + 2 + 1 + 1	Joints 2 and 3	Joints 2 and 3	Joint 1	Joint 3(2)
	Joints 2 and 3	Joints 1 and 3(2)	Joint 1	Joint 3(2)

Note: Joints 1, 2 and 3 in Table 3 denote hip 1 joint, hip 2 joint and knee joint, respectively.

leg 2 are actuated joints; either knee joint or hip 2 joint in leg 4 is actuated joint.

4.2.2 Forward displacement analysis

Once choosing suitable actuators for the parallel manipulator, forward displacement analysis is carried out in the following part.

The coordinate systems established in forward displacement analysis are the same as the coordinate systems built in inverse displacement analysis, as shown in Fig. 6.

After each of the six non-redundant actuated joints undergoes a certain angular displacement, the center of the body moves from point C to point C′ and the center of hip 1 joint moves from point A_i to point $A_{i'}$. The matrix ${}^{O}\boldsymbol{R}_{C'}$ and the vector ${}^{O}\boldsymbol{P}_{C'}$ specify the orientation and translation

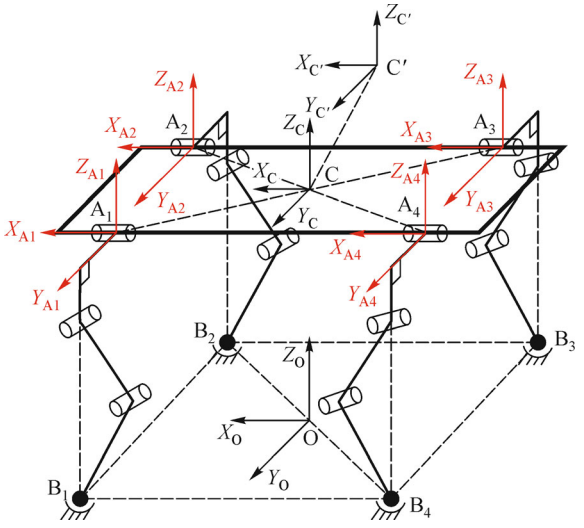

Fig. 6 Four-limb parallel manipulator and coordinate frames

of frame $\{X_{C'}, Y_{C'}, Z_{C'}\}$ with respect to the global frame $\{X_O, Y_O, Z_O\}$, respectively.

Assume that

$$ {}^{O}\boldsymbol{R}_{C'} = \begin{pmatrix} r_1 & r_4 & r_7 \\ r_2 & r_5 & r_8 \\ r_3 & r_6 & r_9 \end{pmatrix}, {}^{O}\boldsymbol{P}_{C'} = \begin{pmatrix} x \\ y \\ z \end{pmatrix} \tag{12} $$

The number of variables in ${}^{O}\boldsymbol{R}_{C'}$ and ${}^{O}\boldsymbol{P}_{C}$ is 12 in total, but the number of independent variables is 6 in consideration of one fact that ${}^{O}\boldsymbol{R}_{C'}$ is a unitary orthogonal matrix. If we want to solve ${}^{O}\boldsymbol{R}_{C'}$ and ${}^{O}\boldsymbol{P}_{C}$, 6 independent equations with respect to r_1–r_9, x, y and z must be found. In the following part, the vector $\overrightarrow{A'_iB_i}$ is expressed using the inverse and forward displacement analysis in order to obtain equations with respect to r_1–r_9, x, y and z.

Using the coordinate transformation, the location of point A'_i in the global frame $\{X_O, Y_O, Z_O\}$ is calculated as

$$ \begin{aligned} {}^{O}\boldsymbol{P}_{A'_i} &= {}^{O}\boldsymbol{R}_{C'}\,{}^{C'}\boldsymbol{P}_{A'_i} + {}^{O}\boldsymbol{P}_{C'} \\ &= {}^{O}\boldsymbol{R}_{C'}\,{}^{C}\boldsymbol{P}_{A_i} + {}^{O}\boldsymbol{P}_{C'} \end{aligned} \tag{13} $$

where ${}^{C'}\boldsymbol{P}_{A'_i} = {}^{C}\boldsymbol{P}_{A_i}$, because the relative posture between the body coordinate and the leg coordinate is not changed when the center of the body moves from point C to point C′.

Considering $\overrightarrow{A'_iB_i} = \overrightarrow{OB_i} - \overrightarrow{OA'_i}$, the vector $\overrightarrow{A'_iB_i}$ with respect to the global frame $\{X_O, Y_O, Z_O\}$ is written as

$$ \begin{aligned} {}^{O}\overrightarrow{A'_iB_i} &= {}^{O}\boldsymbol{P}_{B_i} - {}^{O}\boldsymbol{P}_{A'_i} \\ &= {}^{O}\boldsymbol{P}_{B_i} - ({}^{O}\boldsymbol{R}_{C'}\,{}^{C}\boldsymbol{P}_{A_i} + {}^{O}\boldsymbol{P}_{C'}) \end{aligned} \tag{14} $$

Using the coordinate transformation, the vector $\overrightarrow{A'_iB_i}$ in a new leg frame $\{X_{A'_i}, Y_{A'_i}, Z_{A'_i}\}$ is calculated as

$$ \begin{aligned} {}^{A'_i}\overrightarrow{A'_iB_i} &= ({}^{O}\boldsymbol{R}_{A'_i})^{-1}\,{}^{O}\overrightarrow{A'_iB_i} \\ &= ({}^{O}\boldsymbol{R}_{C'}\cdot{}^{C'}\boldsymbol{R}_{A'_i})^{-1}\,{}^{O}\overrightarrow{A'_iB_i} \end{aligned} \tag{15} $$

In view of the fact that the leg frame is established by translating the body frame from point C to point A_i, it can be obtained as

$$ {}^{C'}\boldsymbol{R}_{A'_i} = {}^{C}\boldsymbol{R}_{A_i} = \boldsymbol{I}_{3\times 3} \tag{16} $$

According to Eqs. (13)–(16), the vector $\overrightarrow{A'_iB_i}$ with respect to the new leg frame $\{X_{A'_i}, Y_{A'_i}, Z_{A'_i}\}$ is found.

$$ {}^{A'_i}\overrightarrow{A'_iB_i} = ({}^{O}\boldsymbol{R}_{C'})^{-1}\Big({}^{O}\boldsymbol{P}_{B_i} - ({}^{O}\boldsymbol{R}_{C'}\,{}^{C}\boldsymbol{P}_{A_i} + {}^{O}\boldsymbol{P}_{C'})\Big) \tag{17} $$

where ${}^{O}\boldsymbol{P}_{B_i}$ and ${}^{C}\boldsymbol{P}_{A_i}$ are only relevant to the initial posture and link parameters of the manipulator; ${}^{O}\boldsymbol{R}_{C'}$ and ${}^{O}\boldsymbol{P}_{C'}$ are the unknown matrices.

Next, the vector $\overrightarrow{A'_iB_i}$ is formulated on the basis of the forward displacement analysis. According to the analysis in Section 3.1, the location of point B_i with respect to the leg frame $\{X_{A'_i}, Y_{A'_i}, Z_{A'_i}\}$ can be calculated with angular displacements of the three revolute joints in the leg i.

$$ {}^{A'_i}\boldsymbol{P}_{B_i} = \begin{bmatrix} -l_3\sin(\theta_{2i}+\theta_{3i}) - l_2\sin\theta_{2i} \\ d\cos\theta_{1i} + \sin\theta_{1i}\Big(l_1 + l_2\cos\theta_{2i} + l_3\cos(\theta_{2i}+\theta_{3i})\Big) \\ d\sin\theta_{1i} - \cos\theta_{1i}\Big(l_1 + l_2\cos\theta_{2i} + l_3\cos(\theta_{2i}+\theta_{3i})\Big) \end{bmatrix} \tag{18} $$

where θ_{1i}, θ_{2i} and θ_{3i} denote the angular displacements of hip 1, hip 2 and knee joints in leg i, respectively.

Considering ${}^{A'_i}\overrightarrow{A'_iB_i} = {}^{A'_i}\boldsymbol{P}_{B_i} - {}^{A'_i}\boldsymbol{P}_{A'_i} = {}^{A'_i}\boldsymbol{P}_{B_i}$, and assuming that ${}^{A'_i}\overrightarrow{A'_iB_i} = \begin{bmatrix} B_{xi} & B_{yi} & B_{zi} \end{bmatrix}^{T}$, it can be derived as

$$ \begin{bmatrix} B_{xi} \\ B_{yi} \\ B_{zi} \end{bmatrix} = \begin{bmatrix} -l_3\sin(\theta_{2i}+\theta_{3i}) - l_2\sin\theta_{2i} \\ d\cos\theta_{1i} + \sin\theta_{1i}\Big(l_1 + l_2\cos\theta_{2i} + l_3\cos(\theta_{2i}+\theta_{3i})\Big) \\ d\sin\theta_{1i} - \cos\theta_{1i}\Big(l_1 + l_2\cos\theta_{2i} + l_3\cos(\theta_{2i}+\theta_{3i})\Big) \end{bmatrix} \tag{19} $$

When θ_{1i}, θ_{2i} and θ_{3i} are all known or partially known, equations with respect to B_{xi}, B_{yi} and B_{zi} can be established according to Eq. (19). Furthermore, the number of equations is equal to the number of known variables, θ_{1i}, θ_{2i} and θ_{3i}. In the whole, six independent equations with respect to B_{xi}, B_{yi} and B_{zi} are built because there are only six actuated joints among twelve joints in four legs. Since B_{xi}, B_{yi} and B_{zi} are varied with r_1–r_9, x, y and z, the previous six equations are also related to r_1–r_9, x, y and z. Based on the six equations and another six equations derived from the unit orthogonal matrix ${}^{O}\boldsymbol{R}_{C'}$, the variables r_1–r_9, x, y and z can be solved correspondingly.

In the forward displacement analysis, it's difficult to build 6 independent equations with respect to B_{xi}, B_{yi} and B_{zi}. In this case, a method for building equations with respect to B_{xi}, B_{yi} and B_{zi} is discussed. According to the analysis in Section 4.2.1, for each leg, there exists 8 cases of actuated joint combinations because each of the three joints is either actuated joint or passive joint. In the case that none of three joints is actuated joint, no equations can be found. In the other seven cases, the method for building equations with respect to B_{xi}, B_{yi} and B_{zi} is proposed as follows.

Case 1: hip 1, hip 2 and knee joints in leg i are all actuated joints, namely, θ_{1i}, θ_{2i} and θ_{3i} are known, B_{xi}, B_{yi} and B_{zi} are calculated as

$$B_{xi} = K_1 \tag{20}$$

$$B_{yi} = K_2 \tag{21}$$

$$B_{zi} = K_3 \tag{22}$$

where

$$K_1 = -l_3\sin(\theta_{2i}+\theta_{3i}) - l_2\sin\theta_{2i};$$

$$K_2 = d\cos\theta_{1i} + \sin\theta_{1i}\left(l_1 + l_2\cos\theta_{2i} + l_3\cos(\theta_{2i}+\theta_{3i})\right);$$

$$K_3 = d\sin\theta_{1i} - \cos\theta_{1i}\left(l_1 + l_2\cos\theta_{2i} + l_3\cos(\theta_{2i}+\theta_{3i})\right).$$

Case 2: hip 2 and knee joints in leg i are actuated joints, that is, θ_{2i} and θ_{3i} are known, Eqs. (23) and (24) are written as

$$B_{xi} = L_1 \tag{23}$$

$$B_{yi}^2 + B_{zi}^2 = d^2 + L_2^2 \tag{24}$$

where, $L_1 = -l_3\sin(\theta_{2i}+\theta_{3i}) - l_2\sin\theta_{2i}$; $L_2 = l_1 + l_2\cos\theta_{2i} + l_3\cos(\theta_{2i}+\theta_{3i})$.

Case 3: hip 1 and knee joints in leg i are actuated joints, namely, θ_{1i} and θ_{3i} are known, Eqs. (25) and (26) can be obtained as

$$B_{yi} + M_1 B_{zi} = M_2 \tag{25}$$

$$(B_{yi} - M_3)^2 + M_4 B_{xi}^2 = M_5 \tag{26}$$

where $M_1 = \tan\theta_{1i}$; $M_2 = d/\cos\theta_{1i}$; $M_3 = d\cos\theta_{1i} + l_1\sin\theta_{1i}$; $M_4 = \sin^2\theta_{1i}$; $M_5 = (l_2^2 + l_3^2 + 2l_2l_3\cos\theta_{3i})\sin^2\theta_{1i}$.

Case 4: hip 1 and hip 2 joints in leg i are actuated joints, that is, θ_{1i} and θ_{2i} are known, Eqs. (27) and (28) can be written as

$$B_{yi} + N_1 B_{zi} = N_2 \tag{27}$$

$$(B_{zi}/\cos\theta_{1i} + N_3)^2 + (B_{xi} + N_4)^2 = l_3^2 \tag{28}$$

where $N_1 = \tan\theta_{1i}$; $N_2 = d/\cos\theta_{1i}$; $N_3 = l_1 + l_2\cos\theta_{2i} - d\tan\theta_{1i}$; $N_4 = l_2\sin\theta_{2i}$.

Case 5: hip 1 joint in leg i is the only actuated joint, namely, only θ_{1i} is known, it can be obtained as

$$B_{yi} + Q_1 B_{zi} = Q_2 \tag{29}$$

where $Q_1 = \tan\theta_{1i}$; $Q_2 = d/\cos\theta_{1i}$.

Case 6: hip 2 joint in leg i is the only actuated joint, that is, only θ_{2i} is known, it can be obtained as

$$B_{xi}^2 + B_{yi}^2 + B_{zi}^2 \pm R_1\sqrt{B_{yi}^2 + B_{zi}^2 - d^2} + R_2 B_{xi} = R_3 \tag{30}$$

where $R_1 = 2(l_1 + l_2\cos\theta_{2i})$; $R_2 = 2l_2\sin\theta_{2i}$; $R_3 = l_3^2 + d^2 - l_1^2 - l_2^2 - 2l_1l_2\cos\theta_{2i}$.

Case 7: the knee joint in leg i is the only actuated joint, namely, only θ_{3i} is known, it can be written as

$$B_{xi}^2 + B_{yi}^2 + B_{zi}^2 \pm 2l_1\sqrt{B_{yi}^2 + B_{zi}^2 - d^2} = S_1 \tag{31}$$

where $S_1 = l_2^2 + l_3^2 + 2l_2l_3\cos\theta_{3i} + d^2 - l_1^2$.

According to the above discussion, six equations with respect to B_{xi}, B_{yi} and B_{zi} which correspond to different combinations of actuated joints are established in order to solve the variables r_1–r_9, x, y and z. Note that the six equations are nonlinear in general cases, so it is difficult to obtain the analytical solutions. Nevertheless, the numerical solutions can be obtained using MATLAB.

4.3 Simulations

4.3.1 Inverse displacement

Based on the coordinates set up in Fig. 4, Table 4 lists the angular displacement of each joint in the body's initial posture. It can be deduced that the center of the body is initially at the location of (0, 0, 150) in the global frame. The planned body position and orientation with respect to the initial body coordinates is shown in Table 5. According to the data in Tables 4 and 5, as well as the inverse displacement analysis in Section 4.1, the angular displacement of each joint is calculated, as shown in Table 6.

By importing the data in Table 6 into the established

Table 4 Angular displacements of all joints in its initial posture

Leg number	Hip 1 joint/rad	Hip 2 joint/rad	Knee joint/rad
1	0	0.94	−1.6143
2	0	−0.94	1.6143
3	0	0.94	−1.6143
4	0	−0.94	1.6143

Table 5 Body position and orientation with respect to the initial body coordinates

Body position and orientation	Value
X-axis rotation (roll)	15°
Y-axis rotation (pitch)	10°
Z-axis rotation (yaw)	15°
X-axis translation	20 mm
Y-axis translation	20 mm
Z-axis translation	−20 mm

Table 6 Results of inverse displacement analysis

Leg number	Hip 1 joint/rad	Hip 2 joint/rad	Knee joint/rad
1	−0.61946	1.12860	−2.1264
2	0.59703	−1.39350	1.8965
3	0.16013	0.87966	−1.7571
4	−0.18813	−0.99065	1.4017

virtual prototype using ADAMS, and setting the angular displacement of each joint as the planned value in Table 6, the body position and orientation with respect to the initial body coordinate can be obtained, as listed in Table 7.

By comparing the data in Table 7 with the data in Table 5, it is obvious that the result in Table 6 is errorless, implying that the inverse displacement analysis in Section 4.1 is also correct.

Table 7 Simulation results using ADAMS

Body position and orientation	Value
X-axis rotation (roll)	15.030°
Y-axis rotation (pitch)	10.354°
Z-axis rotation (yaw)	15.068°
X-axis translation	20.071 mm
Y-axis translation	19.774 mm
Z-axis translation	−19.830 mm

4.3.2 Forward displacement

The six actuators of the parallel manipulator are chosen according to the second feasible combination (in gray) in Table 4. The hip 1, hip 2 and knee joints in leg 1, hip 2 and knee joints in leg 2 and knee joint in leg 4 are actuated joints which angular displacements are shown in Table 6.

According to the forward displacement analysis in Section 4.2, six independent equations with respect to r_1–r_9, x, y and z are established on the basis of Eqs. (20)–(24) and (31). Another six equations can be found in terms of the unitary orthogonal matrix ${}^{O}\boldsymbol{R}_{C'}$. Using MATLAB, 16 numerical solutions are obtained and 8 among them are real solutions. The body position and orientation with respect to the global coordinate are listed in Table 8.

Note that the fourth and seventh solutions in Table 8 are essentially identical to the data in Table 7, implying that the forward displacement analysis in Section 4.2 is correct.

5 Motion capability analysis

The results of the inverse and forward displacement analysis can be not only verified by simulations of virtual prototype. What is more important, all of them can be also used to obtain the workspace and plan the motion of the body.

5.1 Translation capability

Theoretically, the forward displacement analysis can be used to obtain the workspace of the parallel manipulator. However, the period of solving the body position and orientation once is usually very long (greater than 90 seconds). Moreover, the correct solution must be picked from many solutions by using a special algorithm. Therefore, it is rather difficult to determine the workspace of parallel manipulator using the forward displacement analysis.

On the contrary, we may try to calculate the workspace in terms of the inverse displacement analysis. Firstly, the possible workspace can be found on the basis of the geometry of the mechanisms. Next, the possible workspace is meshed. Thus the angular displacement of each joint corresponding to every node can be found. Some nodes are excluded from the real workspace because each joint has a certain range of angular displacement. Finally, the workspace can be obtained by fitting all the nodes belonging to the real workspace. In the first meshing, the meshes may be rough. In the subsequent meshing, the meshes may be smaller because the workspace obtained in the last solving is smaller. Finally, the exact workspace can be determined as the time is constant.

As shown in Fig. 7(a), the workspace of translational motion is obtained using the inverse displacement analysis. In Fig. 7(a), there are two irregular surfaces and the space between the two irregular surfaces is the workspace of the parallel manipulator. Note that the angular displacement of each joint belongs to a certain range because of the interference of the part in the prototype. The angular

Table 8 Numerical solutions using MATLAB

Solution number	*X*-axis rotation /(°)	*Y*-axis rotation /(°)	*Z*-axis rotation /(°)	*X*-axis translation /mm	*Y*-axis translation /mm	*Z*-axis translation /mm
1	−8.6092	−53.5960	25.437	−48.030	20.001	−26.594
2	−13.7780	−59.0860	29.745	−44.272	20.001	−42.933
3	10.7380	−6.0426	14.854	−13.585	20.001	100.314
4	15.0020	10.0010	15.003	20.005	20.001	130.004
5	−13.7780	−59.0860	29.745	−44.272	20.001	−42.933
6	10.7380	−6.0426	14.854	−13.585	20.001	100.314
7	15.0020	10.0010	15.003	20.005	20.001	130.004
8	−8.6092	−53.5960	25.437	−48.030	20.001	−26.594

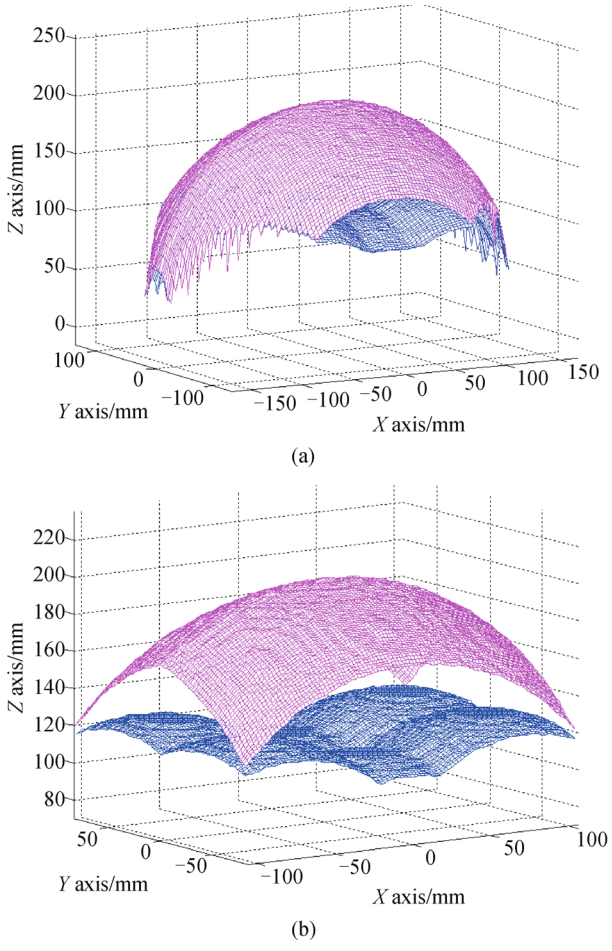

Fig. 7 Workspace resulted by the translational motion. (a) Workspace without considering stability; (b) workspace considering stability

displacement of hip 1 joint in leg i satisfies the condition of $\theta_{1i} \in (-60°,60°)$; the angular displacement of hip 2 joint in leg i satisfies the condition of $\theta_{2i} \in (-95°,95°)$; the angular displacement of knee joint in leg i satisfies the condition of $\theta_{3i} \in (-130°,130°)$.

Note that all feet of the robot are not really constrained to the ground, the stability region of MANA is limited and the ground cannot generate reaction forces in any direction, which results in MANA's smaller workspace. Therefore, taking the stability of the robot into account, its actual workspace is surely smaller, as shown in Fig. 7(b).

5.2 Range of rotation

After the center of the body arrives at a certain position, the rotation capability of the body becomes one issue we are interested in. The rotational range can be also calculated by means of the inverse displacement analysis.

It can be deduced that the center of the body is initially at the location of (0, 0, 150) in the global frame from Table 4. The rotational range of the body is calculated, as shown in Table 9. The angular displacement of each joint belongs to a certain range, as elaborated in Section 5.3.

5.3 Motion planning

Table 9 Angular displacement of the body rotation

	Minimum value/(°)	Maximum value/(°)
X-axis rotation	−52	52
Y-axis rotation	−27	27
Z-axis rotation	−49	49

5.3.1 Plan a helical trajectory

Based on the coordinates set up in Fig. 4, it can be deduced that the center of the body is initially at the location of (0, 0, 150) in the global frame. First, the center of the body translates 50 mm along *X*-axis and moves to the point (50, 0, 150). Then, the center of the body translates along helical trajectory whose radius is 50 mm and pitch is 10 mm for three circles. The center arrives at the point (50, 0, 180). Finally, the center of the body translates -50 mm along *X*-axis and moves to the point (0, 0, 180).

According to the inverse displacement analysis in

Section 4.1, the angular displacement of each joint which corresponds to the planned trajectory can be calculated. The angular displacement can be imported into the established virtual prototype using ADAMS. After the simulation is finished, the related data can be obtained. The resultant simulation trajectory and the theoretical trajectory are depicted using MATLAB. As shown in Fig. 8, a red solid line denotes the theoretical trajectory; a blue dashed line denotes the simulation trajectory obtained under the condition that constraint between the foot and the ground is a pure rolling; green "+" line denotes the simulation trajectory, assuming that all constraints between the foot and the ground are spherical joints.

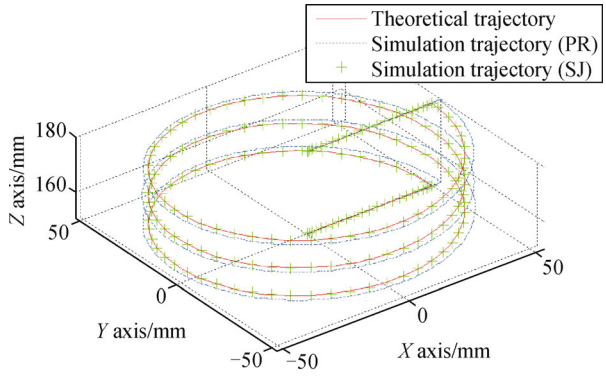

Fig. 8 Comparisons of simulation trajectory and theoretical trajectory

5.3.2 Plan a combined translation and rotation

Based on the coordinates set up in Fig. 4, it can be deduced that the center of the body is initially at the location of (0, 0, 150) in the global frame. First, let the body translate 40, 30 and 30 mm along X, Y and Z axis direction, respectively. Then the body rotates 20°, 20° and 20° around X, Y and Z axis direction, respectively. Note that all displacements and angular displacements are the sine function of time. Both the theoretical curve and simulation curve of translation are depicted in Fig. 9 and the theoretical curve and simulation curve of rotation are drawn in Fig. 10. In these two figures, red solid lines denote the theoretical curves; blue dashed lines mean the simulation curves obtained under the condition that the constraint between the foot and the ground is a pure rolling; green "+" lines denote the simulation curves obtained under the condition that the constraint between the foot and the ground is a spherical joint.

5.3.3 Discussions

By comparisons of the theoretical analysis with the simulation results, it can be concluded that the simulation result is basically the same as the prescribed motion,

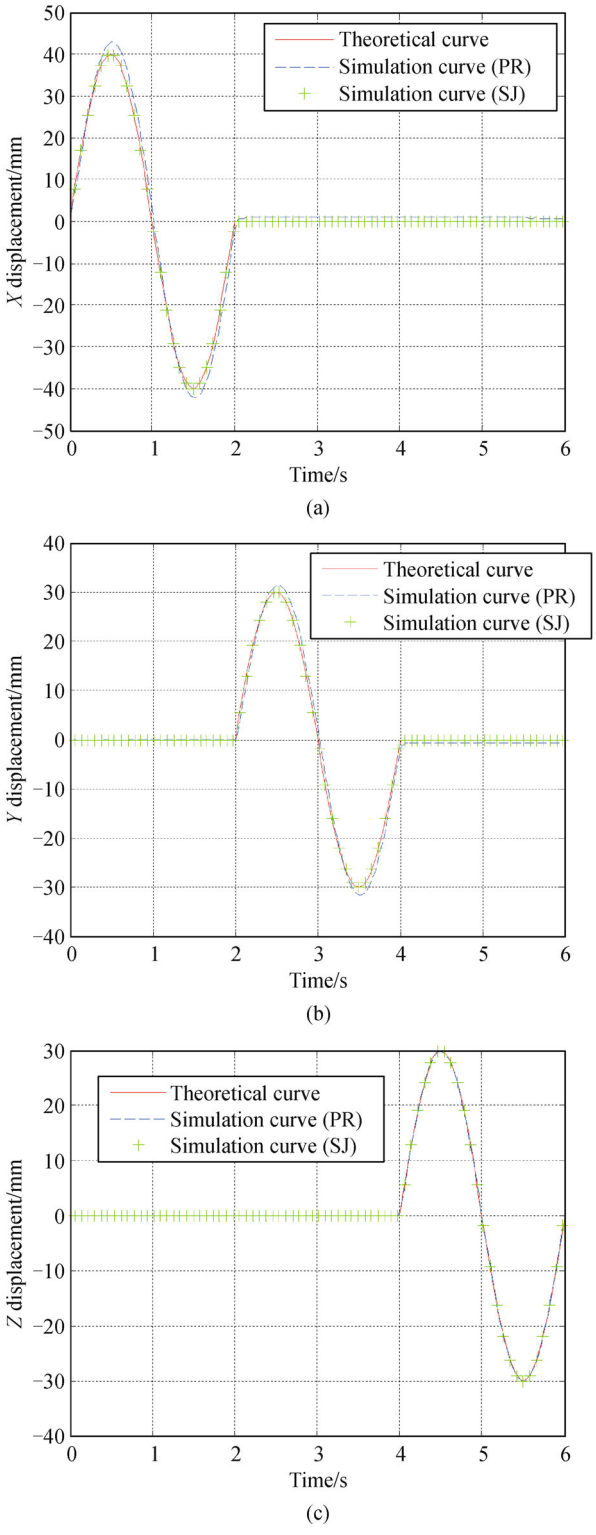

Fig. 9 Variation of the translational displacement with respect to time. (a) Variation of the X-axis translational displacement with respect to time; (b) variation of the Y-axis translational displacement with respect to time; (c) variation of the Z-axis translational displacement with respect to time

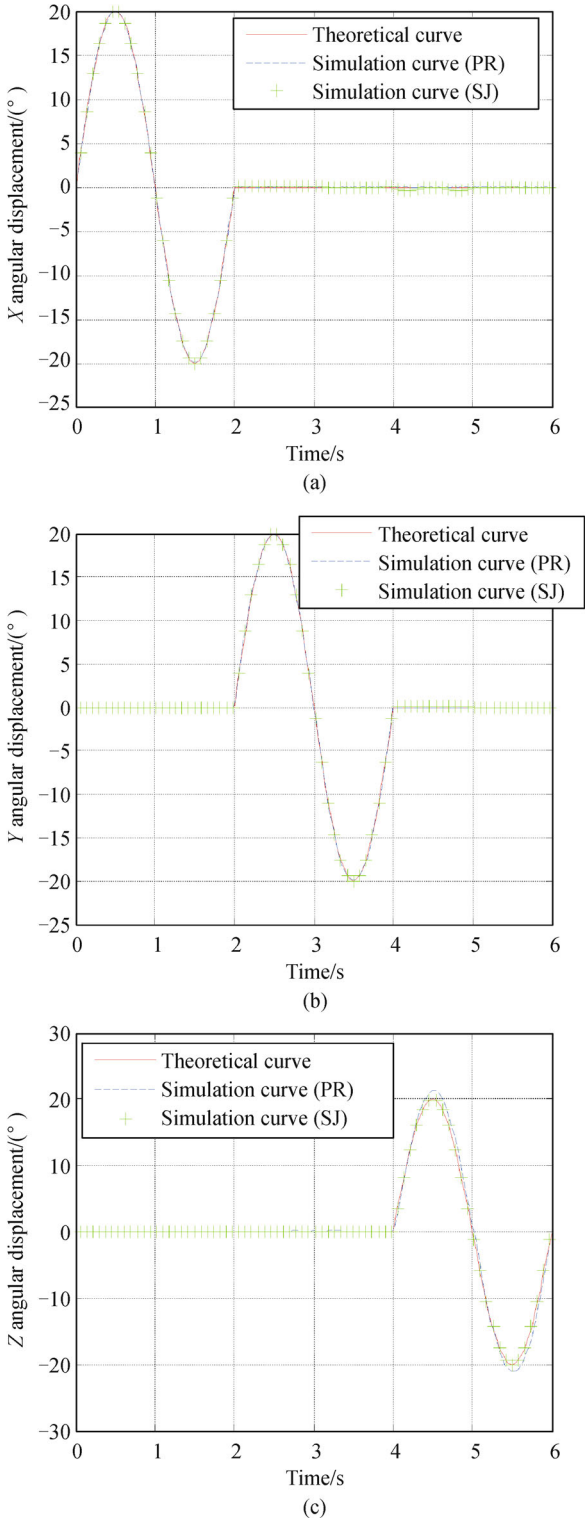

Fig. 10 Variation of the angular displacement with respect to time. (a) Variation of the *X*-axis angular displacement with respect to time; (b) variation of the *Y*-axis angular displacement with respect to time; (c) variation of the *Z*-axis angular displacement with respect to time

implying that the motion planning in terms of parallel kinematics is feasible. Under the condition that the constraint between the foot and the ground is a spherical joint, the simulation result is the identical as the theoretical analysis, implying that the inverse displacement analysis in Section 4.1 is correct. While on the condition that the constraint between the foot and the ground is a pure rolling, the simulation result is also near to the theoretical analysis, implying that it's reasonable to regard the contacting point as a spherical joint during the formulation of parallel kinematics.

6 Conclusions

In this paper, the kinematics and motion capability of a quadruped robot in quadruple stance phase, regarded as a 4-SRRR parallel manipulator, is formulated and afterward simulated. In the forward displacement analysis, a method based on different combinations of actuated joints is put forward. The comparison of the theoretical results and simulation results demonstrates the validity of the approach. The workspace of the parallel manipulator is obtained by using the inverse displacement analysis and has been verified node by node from roughness to exactness. In terms of the inverse displacement analysis, two types of motions, i.e., a helical trajectory and a combined translation and rotation, also two possible motion patterns of a general manipulator, are accomplished. ADAMS simulation results are nearly the same as the planned motions, implying that the robot has a potential to realize desired motion as a parallel manipulator.

Acknowledgements The authors gratefully acknowledge the financial support of the NSFC (Grant Nos. 51175011, 51175010 and 51275552).

References

1. Li Y, Li B, Ruan J, et al. Research of mammal bionic quadruped robots: A review. In: Proceedings of the 2011 IEEE International Conference on Robotics, Automation and Mechatronics (RAM). Qingdao, 2011, 166–171
2. Rutishauser S, Sprowitz A, Righetti L, et al. Passive compliant quadruped robot using central pattern generators for locomotion control. In: Proceedings of the 2nd IEEE/RAS-EMBS International Conference on Biomedical Robotics and Biomechatronics. Scottsdale, 2008, 710–715
3. Kim J S, Park J H. Development of quadruped robot "Hunter" and simulation of its dynamic gaits. In: Proceedings of 2010 IEEE/ASME International Conference on Advanced Intelligent Mechatronics (AIM). Montreal, 2010, 664–669
4. Remy C D, Baur O, Latta M, et al. Walking and crawling with ALoF: A robot for autonomous locomotion on four legs. Industrial Robot: An International Journal (Toronto, Ont.), 2011, 38(3): 264–268
5. Fukuoka Y, Kimura H, Cohen A H. Adaptive dynamic walking of a quadruped robot on irregular terrain based on biological concepts.

International Journal of Robotics Research, 2003, 22(3–4): 187–202

6. Murphy M P, Saunders A, Moreira C, et al. The LittleDog robot. International Journal of Robotics Research, 2011, 30(2): 145–149
7. Raibert M, Blankespoor K, Nelson G, et al. BigDog, the rough-terrain quadruped robot. In: Proceedings of the 17th World Congress: The International Federation of Automatic Control. Seoul, 2008, 10823–10825
8. Ren P, Hong D. Triple stance phase displacement analysis with redundant and non-redundant sensing in a novel three-legged mobile robot using parallel kinematics. Journal of Mechanisms and Robotics, 2009, 1(4): 041001
9. Yu J, Zhang Z, Pei X. Motion pattern planning of a quadruped robot based on parallel kinematics. In: Proceedings of the ASME 2013 International Design Engineering Technical Conferences & Computers and Information in Engineering Conference. Portland, 2013, V06BT07A053
10. Murray R M, Li Z X, Sastry S S. A Mathematical Introduction to Robotic Manipulation. Florida: CRC press, 1994
11. Hopkins J B, Culpepper M L. Synthesis of multi-degree of freedom, parallel flexure system concepts via freedom and constraint Topology (FACT)—Part I: Principles. Precision Engineering, 2010, 34(2): 259–270